Modeling and Simulation of GNSS-R Observables With Effects of Swell

Bowen Li, Lei Yang, Bo Zhang, Dongkai Yang, and Di Wu

***Abstract*—Global navigation satellite system-reflectometry (GNSS-R) has attracted much attention in remote sensing, such as sea wind speed detection, soil moisture, and sea ice. In order to verify the algorithm of GNSS-R, the simulation of GNSS-R plays an important role in this research field. Delay waveform (DW) and delay-Doppler map (DDM) are the main observables in GNSS-R simulation, and are usually effects by the complex ocean environment, such as wind and swell. Besides the effects of wind, this article focuses on analyzing the influence of swell on the simulation of GNSS-R. In this article, a complex model of DW and DDM is presented with effects of swell. Swell modeled here by narrow-band Gaussian spectrum, and the influence of swell on the sea surface scattering coefficient, which can be calculated using Kirchhoff approximation-geometric optics. Observables obtained from the simulation in the space-borne scene are analyzed. The simulation results show that swell has a stable and significant impact on the simulation of GNSS-R observables. Compared with models under no consideration of swell, the model with effects of swell has higher accuracy.**

***Index Terms*—Global navigation satellite system reflectometry (GNSS-R), model, observable, simulation, swell.**

I. Introduction

GLOBAL navigation satellite system-reflectometry (GNSS-R) has become a new branch in the field of remote sensing. Since Hall and Cordey's work on multistatic scatterometry in 1988 [1], and Martin-Neira proposed passive reflectometry and interferometry system (PARIS) in 1993 [2], GNSS-R technology, which use global navigation satellite system (GNSS) reflected signals to detect reflective surface, has been developed rapidly. It is widely used in areas, such as sea state, tide retrieval, sea ice detection, soil moisture, and typhoon/storm/cyclone [3]–[13].

There are two GNSS-R measurement techniques from waveforms using a biantenna receiver or from SNR with conventional mono-antenna receivers [14]. The simulation of waveforms plays an important role in this technique. In 2000, Zavorotny and Voronovich proposed the bistatic scattering model [15], which is mostly used in GNSS-R simulations (Z–V model). Until now, it has proposed various models and simulation methods [16]. Such as, an effective algorithm based on Z–V model to simplify the computational complexity [17], an improved optical approximation model to simulate the scattering power of GNSS reflected signals [4], a stochastic model based on finite time series of the correlation power of GNSS reflected signals [18], a statistical model, and simulator of ocean-reflected GNSS signals [16].

In 2009, in order to perform performance analysis on the PARIS plan and the passive advance unit (PAU) project, the European Space Agency (ESA) developed an end-to-end simulation platform (PAU/PARIS end-to-end performance simulator, P^2EPS) based on the Z–V model [19]. For purpose of the follow-up research, the ESA expanded the function of the P^2EPS system [20]. For GNSS reflectometry, radio occultation, and scatterometry onboard the International Space Station (GEROS-ISS) project, the GEROS-SIM system was developed based on the P^2EPS system [21]. In December 15, 2016, NASA has launched the Cyclone Global Navigation Satellite System constellation to detect tropical hurricane sea surface winds through remote sensing equipment of GNSS reflected signals carried on eight tiny satellites [22]. Correspondingly, NASA has developed its own end-to-end simulation system [23], and used this system for a series of algorithm design and performance simulation [24]–[27]. In addition, there are some other software tools for GNSS-R simulation, such as SAVERS [28] and WAVPY [29].

However, most of the wave spectrum used in the previous research is wind-driven spectrum, such as Elfouhaily spectrum [30]. This means that only the effect of wind on the sea surface roughness is considered. However apart from the wind, there are many other factors, such as swell that may affect the roughness of the sea surface, then affect the scattering of the GNSS reflected signal consequently [31]. At present, there have some studies on the impact of swell on GNSS-R technology. Ghavidel *et al*. have studied the effects of swell on electromagnetic bias [31]. Some scholars have found the existence of swell effects in the low wind speed data of the TechDemoSat-1 [32], [33]. Actually, the scatter of signals is significantly affected by swell at *L*-band [34], which is of great importance in the GNSS-R simulation. Clarizia have studied the superposition of the wave spectrum with the swell [35]. Chen-Zhang *et al*. have modeled long-wave (swell) effects on radar measurements [36]. However, there are few researches on the effects of swell on the simulation of GNSS-R.

Manuscript received March 2, 2020; revised April 4, 2020 and April 26, 2020; accepted April 28, 2020. Date of publication May 4, 2020; date of current version May 15, 2020. This work was supported by the National Natural Science Foundation of China under Grants 41774028 and 31971781. *(Corresponding author: Lei Yang.)*

Bowen Li, Bo Zhang, Dongkai Yang, and Di Wu are with the School of Electronic and Information Engineering, Beihang University, Beijing 100191, China (e-mail: libwab@163.com; bozhang@buaa.edu.cn; edkyang@buaa.edu.cn; wd941127@163.com).

Lei Yang is with the School of Electronic and Information Engineering, Beihang University, Beijing 100191, China, and also with the College of Information Science and Engineering, Shandong Agricultural University, Tai'an 271000, China (e-mail: yanglei@sdau.edu.cn).

Digital Object Identifier 10.1109/JSTARS.2020.2992037

In this article, in order to make the simulation results of GNSS-R more consistent with the real scene, the effects of swell are considered in the simulation of GNSS-R delay waveform (DW) and delay-Doppler map (DDM). The model of GNSS-R observables with the effects of swell is built based on the analysis of swell spectrum. The simulation results are used to analyze the feasibility and accuracy of the proposed model.

The rest of this article is organized as follows. Section II presents a description of the proposed GNSS-R model. Sections III and IV provide the simulation results. Section V compares the simulated results with spaceborne data. At last, Section VI concludes this article.

II. GNSS-R Model With Swell

The numerical simulation of dynamic random sea surface is based on the wind-driven wave spectrum, as well as the simulation of GNSS-R. However, sea surface roughness is not only affected by wind. Swell is wind-driven wave spreading from other areas in the distance, and it also affects the roughness of the sea surface in the local area. Therefore, considering with the effects of swell, a new model for the simulation of GNSS-R observables is presented.

The GNSS reflected signals received by the receiver can be regarded as the weighted sum of the scattering signals of all scattering targets [15]. Assuming that the random phases of each scattered signals in their scattering targets are independently distributed, the expression of the correlation power of the GNSS reflected signals is

$$\left\langle |Y(\tau,f)|^2 \right\rangle = \frac{\lambda^2 P_t G_t {T_c}^2}{(4\pi)^3} \int \frac{G_{r\_x,y}\sigma_{p,q\_x,y}}{R_{t\_x,y}^2 R_{r\_x,y}^2} \Lambda^2 \times \left(\tau - \frac{R_{r\_x,y}+R_{t\_x,y}}{c}\right) S^2(f_{x,y}-f)\mathrm{dxdy} \quad (1)$$

where τ is the delay, f is the satellite frequency (GPS L1 in simulation), $f_{x,y}$ is the frequency reflected by the target, P_t is the transmitter power, G_t is the transmitting antenna gain, λ is the navigation signal wavelength, T_c is the coherent integration time (1 ms in simulation), $G_{r\_x,y}$ is the receiving antenna gain on the scattering target $S_{x,y}$, σ_{p,q_xy} is the bistatic radar cross section (including the reflection coefficient) of the scattering target $S_{x,y}$ when p polarized incident wave corresponds to the q polarized reflected wave, $R_{t\_x,y}$ and $R_{r\_x,y}$ represent the distance between the GNSS satellite and the receiving antenna to the scattering target $S_{x,y}$, respectively, Λ is the autocorrelation function of pseudorandom code, and S is the Doppler filter function.

In order to simulate the GNSS-R observables with effects of swell, the scattering coefficient of the scattering target $(\sigma_{p,q\_x,y})$ should be the superposition of the effects of wind and swell. A large number of researchers have studied electromagnetic scattering of sea surface from analytical method and numerical simulation, such as Kirchhoff approximation-geometric optics (KA-GO), small perturbation method (SPM), small slope approximation, and two-scale model (TSM) [37]. The TSM divides the sea surface into large- and small-scale roughness, where the large-scale is calculated by KA-GO, and the small-scale can be calculated by SPM. The scattering coefficient of TSM can be expressed as

$$\sigma_{\mathrm{TSM}} = \sigma_{\mathrm{KA\text{-}GO}} + \sigma_{\mathrm{SPM}} \quad (2)$$

where $\sigma_{\mathrm{KA\text{-}GO}}$ is the scattering coefficient of large-scale surface roughness, and σ_{SPM} is the scattering coefficient of small-scale surface roughness. The cutoff wavenumber for limiting the wavelength range of the surface waves to distinguish large- and small-scale is given as [38]

$$K_{\mathrm{cutoff}} = \frac{2\pi\cos\theta}{3\lambda} \quad (3)$$

where θ is the angle of incidence and λ is the navigation signal wavelength. According to (3), the cutoff wavenumber of GNSS signal can be obtained. The wavenumber of spectrum, which is less than the cutoff wavenumber, is large-scale, and vice versa.

The most straightforward method for calculating the scattering coefficient is to use the scattering spectrum. The scattering coefficient of wind can be obtained by wind-driven spectrum as an example [30]. Most of the time, wind-driven waves and swell are coexisting. The swell-driven spectrum has been proposed based on narrow-band Gaussian spectrum [34]

$$S_S(k_x,k_y) = \frac{\langle h^2\rangle}{2\pi\sigma_x\sigma_y} \times \exp\left\{-\frac{1}{2}\left[\left(\frac{k_x-k_{xm}}{\sigma_x}\right)^2 + \left(\frac{k_y-k_{ym}}{\sigma_y}\right)^2\right]\right\} \quad (4)$$

where $\langle h^2\rangle$ is the height variance of the swell, σ_x and σ_y are the spectral standard deviations (SDs), and k_x and k_y are the x and y components of the wave number k, respectively. k_{xm} and k_{ym} are the spectral peak wave numbers of the swell in the x and y directions, respectively. The height variance of swell is generally 4 m^2, and the wavelength λ_s of swell is about 50–300 m.

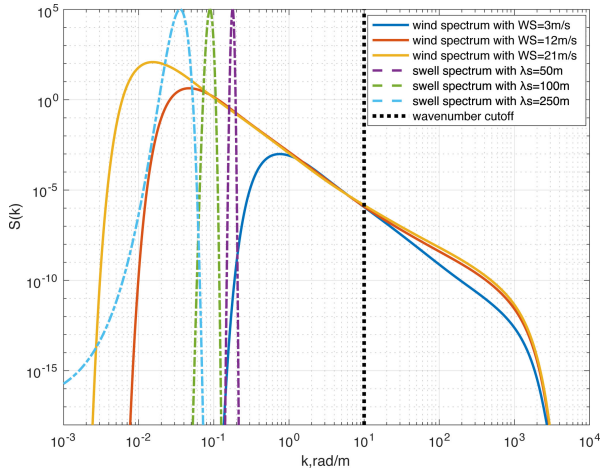

Fig. 1. Wind-driven Eifouhaily spectrum at 3, 12, and 21 m/s wind speed, swell-driven spectrum for 50, 100, and 250 m wavelength, and the cutoff wavenumber of GNSS signal. $S(k)$ is the omnidirectional elevation spectrum.

Fig. 1 shows the wind-driven spectrum at 3, 12, and 21 m/s wind speed, swell-driven spectrum for 50, 100, and 250 m wavelength, and the cutoff wavenumber of GNSS signal. The swell

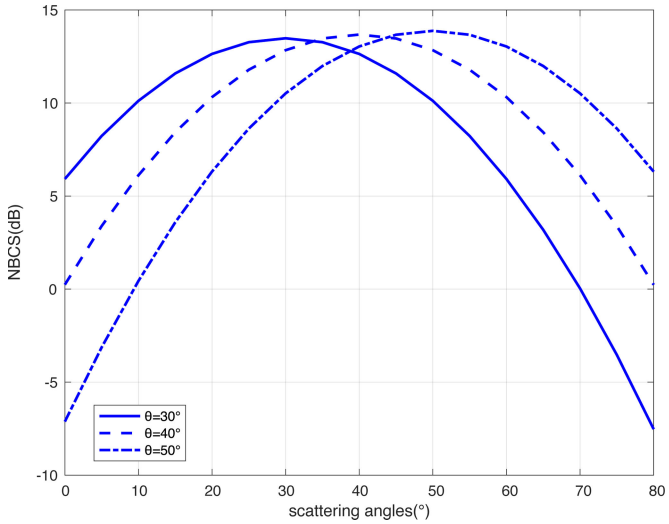

Fig. 2. NBCS between different incidence angles θ and scattering angles.

mainly affects the low wavenumber part of the spectrum, and the swell forms large-scale roughness with great influence on the mirror scattering of GNSS signals. So, the scattering coefficient of swell-driven spectrum can be calculated by KA-GO. The KA-GO model can be expressed as [15]

$$\sigma_{\text{swell,KA-GO}} = \pi|\Re|^2 \frac{|\mathbf{q}|^4}{q_z^4} P_{\text{pdf}}\left(-\frac{q_\perp}{q_z}\right) \tag{5}$$

where $\Re$ is the Fresnel reflection coefficient, and $\mathbf{q}$ is the scattering vector. q, q_z, and $q_\perp$ denote the modulus of the scattering vector $\mathbf{q}$, the modulus of the normal component of $\mathbf{q}$, and the modulus of the horizontal component of $\mathbf{q}$, respectively. P_{pdf} represents the probability distribution of the mean square slope (MSS) of the sea surface, and it can be calculated using a wave spectrum. By assuming a zero-mean Gaussian distribution, the MSS of the sea can be calculated using the wave spectrum model under the influence of swell as

$$\text{MSS} = \int_0^{K_{\text{cutoff}}} k^2 S(k) dk \tag{6}$$

where k represents the wave number of the incident wave, $S(k)$ is the composite wave spectrum considering the influence of the swell, and K_{cutoff} is the cutoff wave number of large-scale roughness.

Since the swell is also caused by wind, the swell has similar characteristics with wind wave as mechanical wave. Therefore, the scattering coefficient of the scattering target $(\sigma_{p,q\_x,y})$ is the superposition of scattering coefficients of wind and swell, and it can be expressed as

$$\sigma_{p,q\_x,y} = \sigma_{\text{wind,TSM}} + \sigma_{\text{swell,KA-GO}} \tag{7}$$

where $\sigma_{\text{wind,TMS}}$ and $\sigma_{\text{swell,KA-GO}}$ are the scattering coefficients of wind-driven spectrum and swell-driven spectrum, respectively. Fig. 2 gives the normalized bistatic-radar cross section (NBCS) between incidence angle θ and scattering angles. From Fig. 2, we can see that NBCS is maximum when the incidence angle is equal to the scattering angle. The improved model of GNSS-R with effects of swell can be obtained by combining (1) and (7).

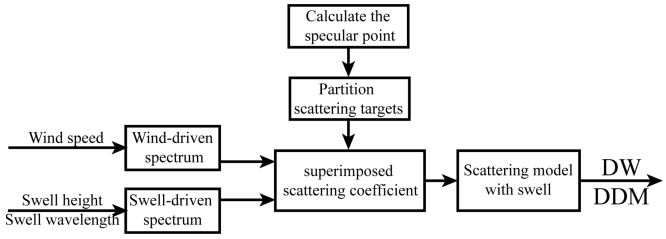

Fig. 3. Processing chain of the simulation.

III. Basic Simulation and Verification

According to the model of GNSS reflected signals considering the effect of swell established in Section II, the model can be used to simulate and analyze the GNSS observables under the effect of swell.

Assuming that the GNSS reflection event is a spaceborne scene and the geodetic reference is ECEF, the position and velocity of the GNSS satellite set in the simulation environment are [X_s = –11 178 791.991294 m, Y_s = –13 160 191.204988 m, Z_s = 20 341 528.127540 m] and [V_{sx} = 2523.258023 m/s, V_{sy} = –361.592839 m/s, V_{sz} = 1163.748104 m/s], respectively. The position and velocity of the receiver mounted on the satellite is [X_r = –4 069 896.7033860330 m, Y_r = –3 583 236.9637350840 m, Z_r = 4 527 639.2717581640 m] and [V_{rx} = –4738.0742342063 m/s, V_{ry} = –1796.2525689964 m/s, V_{rz} = –5654.9952013657 m/s]. The wind speed of ocean surface is 5 m/s, the height variance of swell is 4 m^2, the wavelength of swell is 250 m, the gain of receiving antenna is 12 dB, and the antenna 3-dB beamwidth is 20°.

Simulations are performed using the proposed GNSS-R model considering the effects of swell. The processing chain of the simulation is shown in Fig. 3. The DW and DDM obtained by the simulation are shown in Fig. 4. It can be seen that the DW and DDM results obtained by the simulation have similar waveform shapes and trends, when considering only the wind, or both the influence of the wind and swell. The DDM has obvious horseshoe characteristics, which meets the laws of typical theoretical DW and DDM waveform. It can be proved that the model of GNSS reflected signals with the effect of swell is feasible.

As shown in Fig. 4(a), swell plays a significant impact on the scattering of GNSS-R signals, and it also can be seen from Fig. 4(b) and (c). The swell forms large-scale roughness with great influence on the mirror scattering of GNSS signals, and the correlation power decreases. By adding the influence factor of swell, the sea surface roughness changes with the correlation power. The swell can increase the sea surface roughness, enhance the diffuse reflection at the reflecting surface, reduce the specular reflection part, and reduce the correlation power significantly. Therefore, the swell is as important as the wind

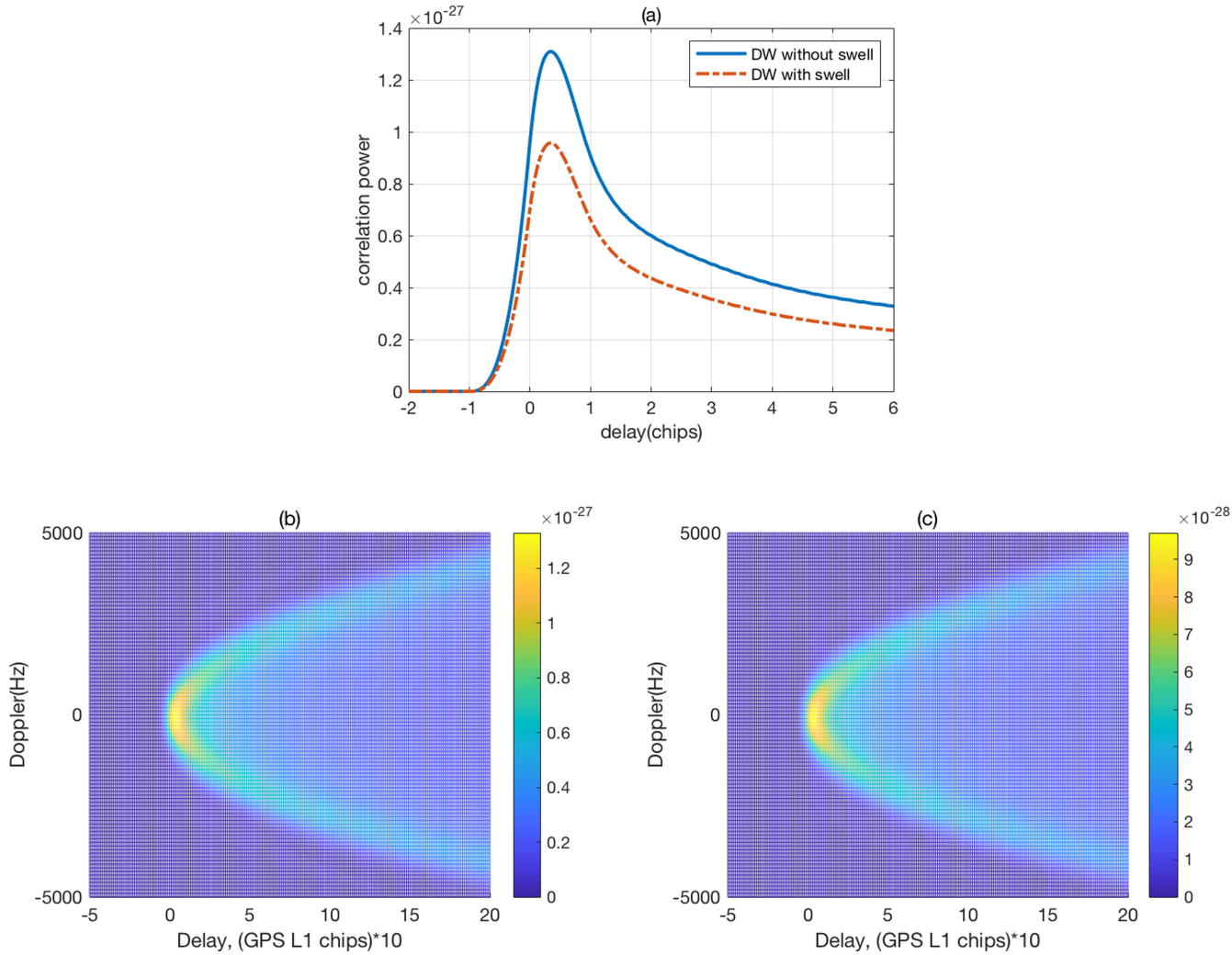

Fig. 4. Simulation results of DW and DDM. (a) DW without and with the effect of swell. (b) DDM without the effect of swell. (c) DDM with the effect of swell.

speed in affection of sea surface roughness, which should be considered in the simulation of GNSS-R observables.

IV. Deep Simulation and Analysis

In order to further analyze the influence of the swell on GNSS-R simulation, different wind speeds are simulated and analyzed. The wind speed is set in the range from 1 to 25 m/s. The DW obtained by the simulation is shown in Fig. 5(a) and (b). It can be seen that with wind speed increase, the correlation power of the simulated DW gradually decreases, which is in line with the theoretical basis of GNSS-R remote sensing. The increase of the wind speed leads to the increase of the sea surface roughness, the decrease of specular reflection, the increase of diffuse reflection, and the significantly decrease of the correlation power.

Fig. 5(c) and (d) show the effects of the swell. Define D is the difference between the peak value (PV) of DW without swell and with swell, R_a is the ratio between the PV of DW with swell and without swell, and R_b and R_c are the ratios between D and the PV of DW without and with swell, respectively. Since in same simulation environment, D is usually caused by the swell. It can be seen from Fig. 5(c) that D is close to a straight line for a constant swell at different wind speeds. No matter how large the wind speed is, the impact of the swell on the sea surface roughness is kept stable. The same conclusion can be found in Fig. 5(d) too. Because the impact of the swell is stable, these three ratios varied smoothly. Therefore, in the simulation of GNSS-R signals, the constant swell will cause a stable effect.

The scattering coefficient of the scattering target can be calculated according to (7). It can be analyzed more precisely under the impact of the swell by numerical calculation. Fig. 6(a) shows the different scattering coefficients of the wind, swell, and both wind and swell, respectively. The red points at a certain wind speed in Fig. 6(a) are the scattering coefficients of different scattering targets caused by wind and the blue circles represent the mean scattering coefficients. The purple asterisks are the mean scattering coefficients of different scattering targets caused by swell. They are close to a straight line at different wind speeds and these values are basically the same. Once again, the impact of the swell on the sea surface roughness is very stable. Fig. 6(b) shows the correlation coefficients of DW with swell and without swell. From Fig. 6(b), it can be seen that the correlation

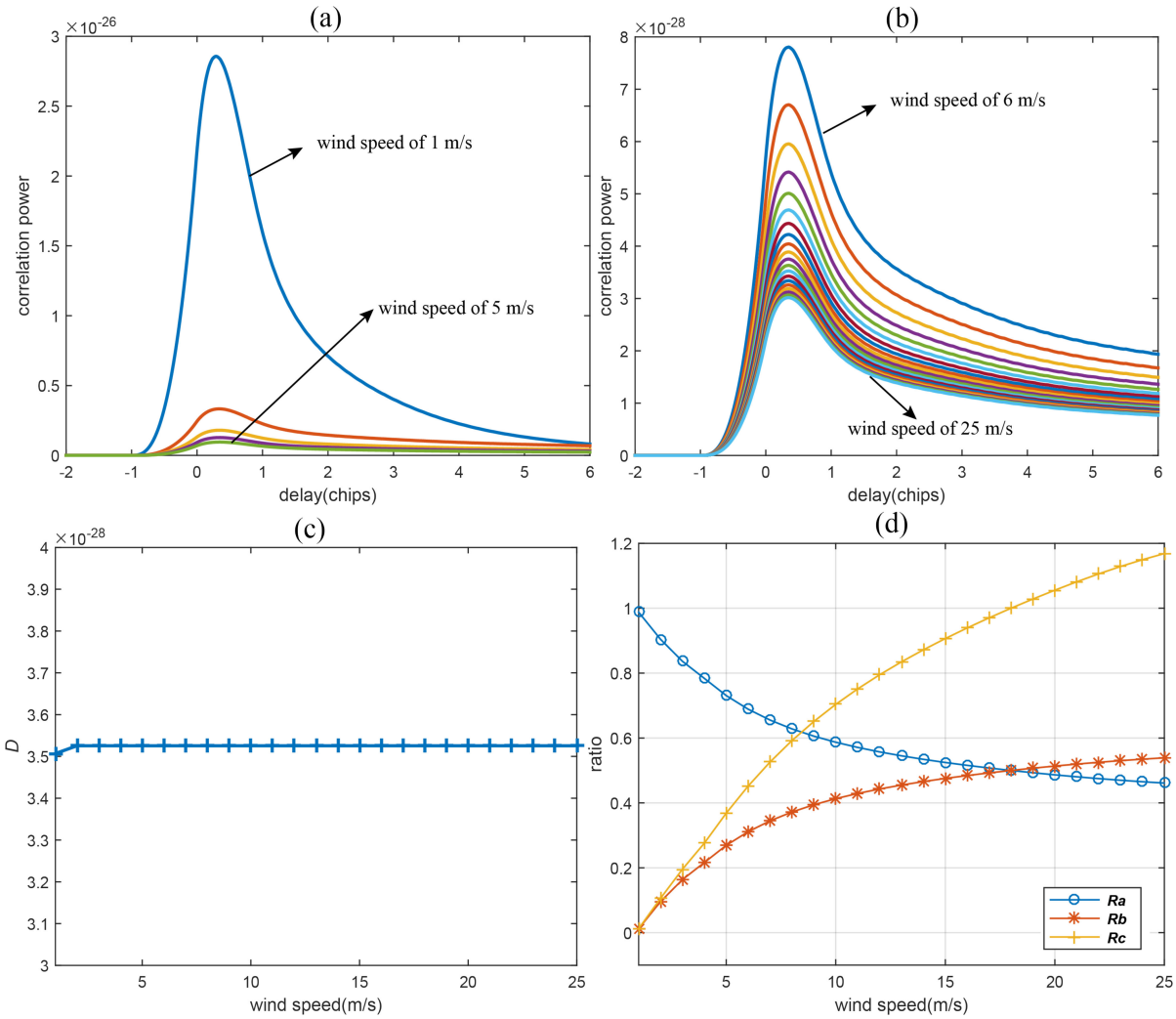

Fig. 5. Simulation results with different wind speeds. (a) DW of wind speed from 1 to 5 m/s. (b) DW of wind speed from 6 to 25 m/s. (c) Difference between the PV of DW with swell and without swell ($\mathrm{PV}_{\mathrm{without\ swell}}$-$\mathrm{PV}_{\mathrm{with\ swell}}$). (d) R_a is $\mathrm{PV}_{\mathrm{with\ swell}}$/$\mathrm{PV}_{\mathrm{without\ swell}}$, R_b is ($\mathrm{PV}_{\mathrm{without\ swell}}$-$\mathrm{PV}_{\mathrm{with\ swell}}$)/ $\mathrm{PV}_{\mathrm{without\ swell}}$, and R_c is ($\mathrm{PV}_{\mathrm{without\ swell}}$-$\mathrm{PV}_{\mathrm{with\ swell}}$)/ $\mathrm{PV}_{\mathrm{with\ swell}}$.

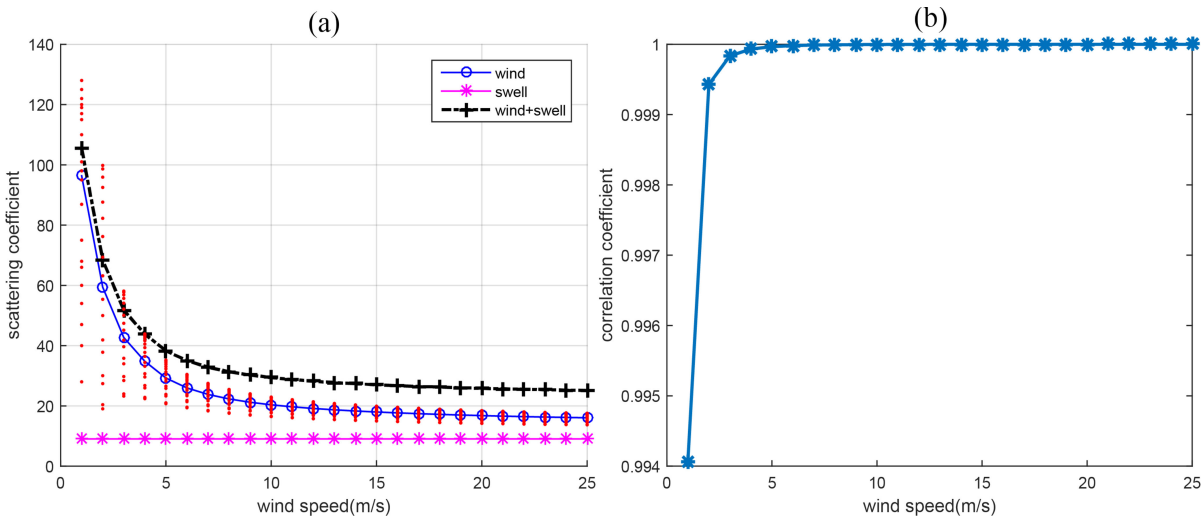

Fig. 6. Simulation results of the scattering coefficient and the correlation coefficient. (a) Scattering coefficients of wind, swell, and both wind and swell. (b) Correlation coefficients of DW with swell and without swell.

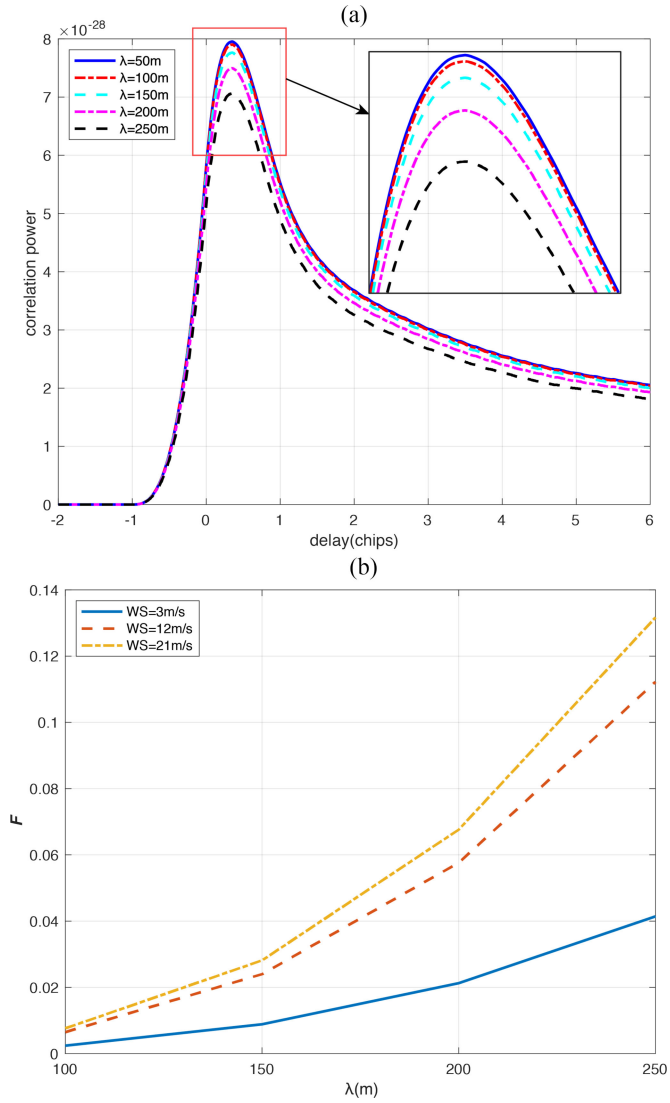

Fig. 7. Simulation results with different swell wavelength. (a) DWs at 12-m/s wind speed with the swell wavelength of 50, 100, 150, 200, and 250 m. (b) Ratio of other swell wavelengths to 50-m swell wavelength at wind speed of 3, 12, and 21 m/s.

coefficients increase as the wind speed increases from 0.994 to 1. The correlation coefficients between DWs gradually converge, and finally converge to 1. In all case, we have a quite perfect correlation.

For different swell, the swell wavelength λ of 50, 100, 150, 200, and 250 m are used for simulation. Fig. 7 shows the simulation results of different swell. At the wind speed of 12 m/s, the DWs obtained by the simulation are as shown Fig. 7(a). It can be seen that at a same wind speed, with the increase of the swell wavelength, the correlation power of the simulated DW gradually decreases. The increase of the swell wavelength leads to the increase of the sea surface roughness, the decrease of specular reflection, the increase of diffuse reflection, and the significantly decrease of the correlation power.

Fig. 7(b) shows the effects of different swell. Using swell wavelength of 50 m as a benchmark, we define F as the ratio

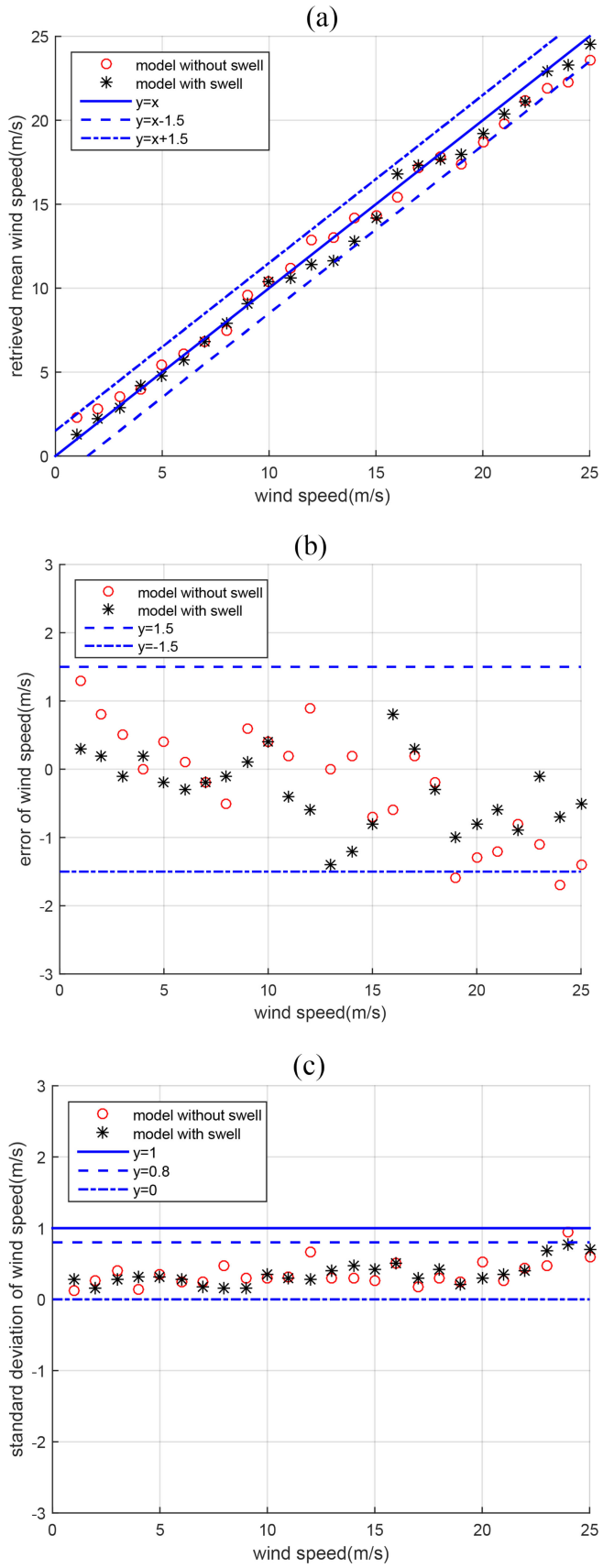

Fig. 8. Scatterplot of the retrieved wind speed of the model without swell and with swell. (a) Retrieved mean wind speed. (b) Error of wind speed. (c) SD of wind speed.

TABLE I
DATA INFORMATION OF UK TDS-1

Style	Detail
Data ID	RD000002/TD000008
Time	2014-09-01 T20:24
Wind speed (m/s)	5
Swell height variance (m^2)	4
Swell wavelength (m)	180
Elevation angle (°)	63.8
Antenna gain (dB)	12

of other swell wavelengths to 50 m wavelength. With the increase of the swell wavelength, the correlation power decreases gradually faster. Compared with the swell wavelength range of [100, 150] m, the range of [200, 250] m has a large impact on correlation power and it can be seen that at different wind speed, the increase of the swell wavelength would have a similar effect. The greater the wind speed, the greater the impact caused by the large swell wavelength.

In addition, observation of sea wind speed is very useful for the verification of simulation results. The wind speed is set from 1 to 25 m/s, and the results are shown in Fig. 8 by retrieving the wind speed with the simulated observables for 80 times. The wind speed retrieval method is the least square method by matching the theoretical correlation power curve. In Fig. 8, the error range of the retrieved mean wind speed is about [–1.5, 1.5] m/s, and the retrieval results meet the requirement of wind speed inversion. However, for the SD, the results of model with swell is about [0, 0.8] m/s. In condition without swell, the SD is about [0, 1] m/s. SD with swell is smaller than SD without swell, and it shows that the retrieval error wind speed of model with swell is smaller. The model with swell has a higher precision. Therefore, the results of the model with swell are better than that without swell.

V. VALIDATION USING SPACEBORNE DATA

In order to validate the proposed model, a comparison between the simulated results and spaceborne data is desirable. A comparative test is made by using the data of UK TDS-1. These data are collected on September 1, 2014. The swell information is got from FY data and ECMWF ERA-5 data. The data information is shown in Table I.

The position and velocity of the GNSS satellite of the ECEF geodetic reference are [X_s = –21 842 415.002320271 m, Y_s = –15 180 714.434890306 m, Z_s = –970 098.63007445715 m] and [V_{sx} = 258.9350681325609 m/s, V_{sy} = –174.18019867283397 m/s, V_{sz} = –3155.3472623290832 m/s], respectively. The position and velocity of the receiver mounted on the satellite are [X_r = –6 806 318.464608931 m, Y_r = –1 262 592.5946520383 m, Z_r = –1 103 923.0938045324 m] and [V_{rx} = 847.56799573840181 m/s, V_{ry} = 1803.7380384723278 m/s, V_{rz} = –7368.059680401838 m/s]. The comparison results of simulated results and spaceborne data are shown in Fig. 9. The height variance of swell is 4 m^2 and the wavelength of swell is 180 m.

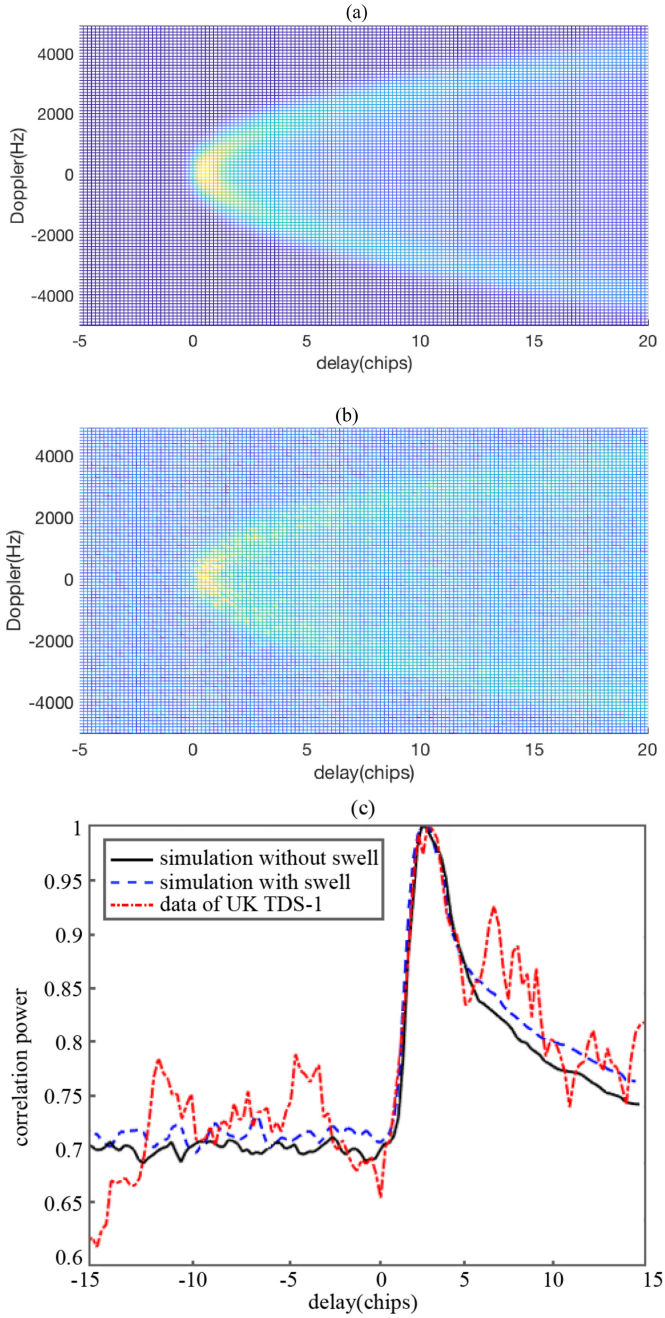

Fig. 9. Comparison result of simulated results and spaceborne data. (a) Simulated DDM of the GNSS-R model with the effects of swell. (b) DDM processed by the UK TDS-1 data. (c) DW of the model with swell, the model without swell, and the UK TDS-1 data.

As shown in Fig. 9(a) and (b), the simulated DDM of the proposed model has a good agreement with the DDM of the UK TDS-1 data. It can be seen from Fig. 9(c) that in the range of [–1, 15] chips, the simulated DW of the proposed model is

TABLE II
COMPARISON RESULTS

Group	Data information		DW		DDM	
	Wind speed (m/s)	Swell wavelength (m)	CC1	CC2	CC3	CC4
1	3.8	140	0.87	0.89	0.93	0.94
2	6.0	220	0.85	0.86	0.96	0.97
3	4.6	190	0.89	0.93	0.95	0.95
4	5.2	110	0.88	0.89	0.92	0.95
5	8.4	160	0.83	0.85	0.93	0.96

closer to the DW processed by the UK TDS-1 data, and the correlation coefficient is reached 0.92. At the same simulation environment, the correlation coefficient between the simulated DW without swell and the DW of the UK TDS-1 data is 0.88. At the same time, the correlation coefficient of real DDM and the DDM of the proposed model is 0.97, the correlation coefficient of real DDM and the DDM of the model without swell is only 0.95. It is significantly lower than the newly proposed model. Therefore, the GNSS-R model considering the effects of swell is not only closer to the real situation at the physical level, but also the accuracy of the simulation has improved. The simulation result of the proposed model shows higher precision to simulate the GNSS-R observables.

At last, more groups of UK TDS-1 data are used for validation at the same steps as earlier. Define CC_1 is the correlation coefficient of real DW and the simulated DW without swell, CC_2 is correlation coefficient of real DW and the simulated DW with swell, CC_3 is the correlation coefficient of real DDM and the simulated DDM without swell, and CC_4 is correlation coefficient of real DDM and the simulated DDM with swell. Table II shows the comparison results of different five groups of UK TDS-1 data and simulated results with and without swell. As shown in Table II, the correlation coefficients of DDMs are higher than that of DWs. From a statistical perspective, considering the effects of swell, the correlation coefficients of DWs are significantly higher than that without swell. For DDMs, the correlation coefficients with swell are not less than that without swell. Therefore, considering the effects of swell will have better simulation results and the results are closer to the real scene.

VI. CONCLUSION

Based on the simulation of swell spectrum, a model of GNSS-R observables considering the effects of swell is proposed. This model calculates the scattering coefficient of the wind and swell by TSM and KA-GO, respectively. The established model is used in multidimensional simulation verification. Swell changes the sea surface roughness and has a significant impact on the scattering of GNSS-R signals. Therefore, the simulation of GNSS-R observables needs to consider the swell as well as the wind speed.

With the increase of the wind speed, the sea surface roughness changes. However, no matter how large the wind speed is, the sea surface roughness caused by the swell changes stably. The proposed model in this article realized a higher precision compared with those models under no consideration of the swell. The comparison results between simulated results and the UK TDS-1 data also proved that. In the future, the simulation of GNSS-R observables taking more impact factors into consideration will be more and more important.

In addition to wind and swell, there are also many factors that may affect the roughness of the sea surface, such as rain, tide, bubble, oceanic surges, and measurement noise. Furthermore, considering more factors in the simulation of GNSS-R observables can make the simulation results more realistic and accurate.

REFERENCES

[1] C. D. Hall and R. A. Cordey, "Multistatic scatterometry," in *Proc. Int. Geosci. Remote Sens. Symp.*, 1988, pp. 561–562.

[2] M. Martin-Neira, "A passive reflectometry and interferometry system (PARIS): Application to ocean altimetry," *ESA J*, vol. 17, no. 4, pp. 331–355, 1993.

[3] W. Li, A. Rius, F. Fabra, E. Cardellach, S. Ribó, and M. Martín-Neira , "Revisiting the GNSS-R waveform statistics and its impact on altimetric retrievals," *IEEE Trans. Geosci. Remote Sens.*, vol. 56, no. 5, pp. 2854–2871, May 2018.

[4] D. R. Thompson, T. M. Elfouhaily, and J. L. Garrison , "An improved geometrical optics model for bistatic GPS scattering from the ocean surface," *IEEE Trans. Geosci. Remote Sens.*, vol. 43, no. 12, pp. 2810–2821, Dec. 2005.

[5] F. Wang, B. Zhang, D. Yang, W. Li, and Y. Zhu, "Sea-state observation using reflected beidou GEO signals in frequency domain," *IEEE Geosci. Remote Sens. Lett.*, vol. 13, no. 11, pp. 1656–1660, Nov. 2016.

[6] Z. Li, C. Zuffada, S. T. Lowe, T. Lee, and V. Zlotnicki , "Analysis of GNSS-R altimetry for mapping ocean mesoscale sea surface heights using high-resolution model simulations," *IEEE J. Sel. Topics Appl. Earth Observ. Remote Sens.*, vol. 9, no. 10, pp. 4631–4642, Oct. 2016.

[7] A. Alonso-Arroyo, V. U. Zavorotny, and A. Camps, "Sea ice detection using U.K. TDS-1 GNSS-R data," *IEEE Trans. Geosci. Remote Sens.*, vol. 55, no. 9, pp. 4989–5001, Sep. 2017.

[8] W. Li, E. Cardellach, F. Fabra, A. Rius, S. Ribo, and M. Martin-Neira, "First spaceborne phase altimetry over sea ice using TechDemoSat-1 GNSS-R signals," *Geophys. Res. Lett.*, vol. 44, no. 16, pp. 8369–78376, 2017.

[9] S. J. Katzberg, O. Torres, M. S. Grant, and D. Nasters, "Utilizing calibrated GPS reflected signals to estimate soil reflectivity and dielectric constant: Results from SMEX02," *Remote Sens. Environ.*, vol. 100, no. 1, pp. 17–28, 2006.

[10] A. Komjathy, V. U. Zavorotny, P. Axelrad, G. Born, and J. Garrison, "GPS signal scattering from sea surface: Comparison between experimental data and theoretical model," in *Proc. IEEE Int. Geosci. Remote Sens. Symp.*, 2000, vol. 7, pp. 2855–2857.

[11] V. U. Zavorotny and A. G. Voronovich, "Bistatic GPS signal reflections at various polarizations from rough land surface with moisture content," in *Proc. IEEE Int. Geosci. Remote Sens. Symp.*, 2000, pp. 2852–2854.

[12] J. S. Thomas and H. R. Haas, "Improving GNSS-R sea level determination through inverse modelling of SNR data," *Radio Sci.*, vol. 58, no. 1, pp. 1286–1296, 2016.

[13] P. L. Vu *et al.*, "Identifying 2010 Xynthia storm signature in GNSS-R-based tide records," *Remote Sens.*, vol. 11, no. 7, 2019, Art. no. 782.

[14] Y. Dongkai, L. I. Xiaohui, and W. Feng, "Analysis of application status of GNSS reflected signal in ocean remote sensing," *Radio Eng.*, vol. 49, no. 10, pp. 843–848, 2019.

[15] V. U. Zavorotny and A. G. Voronovich, "Scattering of GPS signals from the ocean with wind remote sensing application," *IEEE Trans. Geosci. Remote Sens.*, vol. 38, no. 2, pp. 951–964, Mar. 2000.

[16] J. L. Garrison, "A statistical model and simulator for ocean-reflected GNSS signals," *IEEE Trans. Geosci. Remote Sens.*, vol. 54, no. 10, pp. 6007–6019, Oct. 2016.

[17] J. F. Marchan-Hernandez, A. Camps, N. Rodriguez-Alvarez, E. Valencia, X. Bosch-Lluis, and I. Ramos-Perez, "An efficient algorithm to the simulation of delay-Doppler maps of reflected global navigation satellite system signals," *IEEE Trans. Geosci. Remote Sens.*, vol. 47, no. 8, pp. 2733–2740, Aug. 2009.
[18] G. Giangregorio, M. di Bisceglie, P. Addabbo, T. Beltramonte, S. D'Addio, and C. Galdi, "Stochastic modeling and simulation of delay–Doppler maps in GNSS-R over the ocean," *IEEE Trans. Geosci. Remote Sens.*, vol. 54, no. 4, pp. 2056–2069, Apr. 2009.
[19] H. Park *et al.*, "End-to-end simulator for global navigation satellite system reflectometry space mission," in *Proc. IEEE Geosci. Remote Sens. Symp.*, 2010, pp. 4294–4297.
[20] H. Park, A. Camps, D. Pascual, A. Alonso, F. Martin, and H. Carreno-Luengo, "Improvement of the PAU/PARIS end-to-end performance simulator (P2EPS) in prepapation for upcoming GNSS-R missions," in *Proc. IEEE Geosci. Remote Sens. Symp.*, 2013, pp. 362–365.
[21] H. Park, A. Camps, D. Pascual, R. Onrubia, A. Alonso-Arroyo, and F. Martin, "Evolution of PAU/PARIS end-to-end performance simulator (P2EPS) towards GNSS reflectometry, radio occulation and scatterometry simulator (GEROS-SIM)," in *Proc. IEEE Geosci. Remote Sens. Symp.*, 2015, pp. 4757–4760.
[22] C. S. Ruf *et al.*, "The CYGNSS nanosatellite constellation hurricane mission," in *Proc. IEEE Int. Geosci. Remote Sens. Symp.*, 2012, pp. 214–216.
[23] A. O'Brien, "End-to-end simulator technical memo," CYGNSS Official Documentation 148-0123, The Ohio State University, Columbus, OH, USA, 2014.
[24] N. Rodriguez-Alvarez and J. L. Garrison, "Generalized linear observables for ocean wind retrieval from calibrated GNSS-R delay-Doppler maps," *IEEE Trans. Geosci. Remote Sens.*, vol. 54, no. 2, pp. 1142–1155, Feb. 2016.
[25] S. Gleason, C. S. Ruf, M. P. Clarizia, and A. J. O'Brien, "Calibration and unwrapping of the normalized scattering cross section for the Cyclone Global Navigation Satellite System," *IEEE Trans. Geosci. Remote Sens.*, vol. 54, no. 5, pp. 2495–2509, May 2016.
[26] M. P. Clarizia and C. S. Ruf, "Wind speed retrieval algorithm for the Cyclone Global Navigation Satellite System (CYGNSS) mission," *IEEE Trans. Geosci. Remote Sens.*, vol. 54, no. 8, pp. 4419–4432, Aug. 2016.
[27] F. Said, S. Soisuvarn, Z. Jelenak, and P. S. Chang, "Performance assessment of simulated CYGNSS measurements in the tropical cyclone environment," *IEEE J. Sel. Topics Appl. Earth Observ. Remote Sesns.*, vol. 9, no. 10, pp. 4709–4719, Oct. 2016.
[28] N. Pierdicca, L. Guerriero, and R. Giusto, "SAVERS: A simulator of GNSS reflections from bare and vegetated soils," *IEEE Trans. Geosci. Remote Sens.*, vol. 52, no. 10, pp. 6542–6554, Oct. 2014.
[29] F. Fabra, E. Cardellach, W. Li, and A. Rius, , "WAVPY: A GNSS-R open source software library for data analysis and simulation," in *Proc. IEEE Int. Geosci. Remote Sens. Symp.*, 2017, pp. 4125–4128.
[30] T. Elfouhaily, B. Chapron, and K. Katsaros, "A unified directional spectrum for long and short wind-driven waves," *J. Geophys. Res.*, vol. 102, no. C7, pp. 15781–15796, 1997.
[31] A. Ghavidel and A. Camps, "Impact of rain, swell, and surface currents on the electromagnetic bias in GNSS-reflectometry," *IEEE J. Sel. Topics Appl. Earth Observ. Remote Sens.*, vol. 9, no. 10, pp. 4643–4649, Oct. 2016.
[32] M. Unwin, P. Jales, J. Tye, C. Gommenginger, G. Foti, and J. Rosello, "Spaceborne GNSS-reflectometry on TechDemoSat-1: Early mission operations and exploitation," *IEEE J. Sel. Topics Appl. Earth Observ. Remote Sens.*, vol. 9, no. 10, pp. 4525–4539, Oct. 2016.
[33] S. Soisuvarn, Z. Jelenak, F. Said, P. S. Chang, and A. Egido, "The GNSS reflectometry response to the ocean surface winds and waves," *IEEE J. Sel. Topics Appl. Earth Observ. Remote Sens.*, vol. 9, no. 10, pp. 4678–4699, Oct. 2016.
[34] S. L. Durden and J. F. Veseck, "A physical radar cross-section model for a wind-driven sea with swell," *IEEE J. Ocean. Eng.*, vol. 10, no. 4, pp. 445–451, Oct. 1985.
[35] M. P. Clarizia, "Investigating the effect of ocean waves on GNSS-R microwave remote sensing measurements," Ph.D. dissertation, School of Ocean Earth Sci., Univ. Southampton, Southampton, U.K., 2012.
[36] D. D. Chen-Zhang, C. S. Ruf, F. Ardhuin, and J. Park, "GNSS-R nonlocal sea state dependencies: Model and empirical verification," *J. Geophys. Res. Oceans*, vol. 121, no. 11, pp. 8379–8394, 2016.
[37] J. C. Leader, "Incoherent backscatter from rough surfaces: The two-scale model reexamined," *Radio Sci.*, vol. 13, no. 3, pp. 441–457, 2016.
[38] G. S. Brown, "Backscattering from a Gaussian-distributed perfectly conducting rough surface," *IEEE Trans. Antennas Propag.*, vol. AP-26, no. 3, pp. 472–482, May 1978.

Bowen Li received the master's degree in electronic information engineering in 2017 from the School of Electronic and Information Engineering, Beihang University, Beijing, China, where he has been working toward the Ph.D. degree in information and signal processing since 2017.

His research interest focuses on global navigation satellite system reflectometry simulation for Ph.D. degree.

Lei Yang received the bachelor's and master's degrees in computer science from Northwestern Polytechnical University, Xi'an, China, in 2004 and 2008, respectively, and the Ph.D. degree in agricultural electrification and automation from Shandong Agricultural University, Tai'an, China, in 2017.

He is currently an Associate Professor with the College of Information Science and Engineering, Shandong Agricultural University, Tai'an Shandong, China. From 2019, he has been a Postdoctor with Beihang University, Beijing, China. His research interests include GNSS-R and MEMS/ASIC integrated system.

Bo Zhang received the Ph.D. degree in information and communication engineering from the School of Electronic and Information Engineering, Beihang University, Beijing, China, in 2006.

From 2006 to 2009, he has been a Postdoctor of electronic science and technology. Since 2009, he has been a Lecturer with the School of Electronic and Information Engineering, Beihang University. His research interests include global navigation satellite system and spread spectrum communication.

Dongkai Yang was born in China in 1972. He received the B.S. degree in electronic engineering from the North University of China, Taiyuan, China, in 1994, and the M.S. and Ph.D. degrees in communication and information system from Beihang University, Beijing, China, in 1997 and 2000, respectively.

From 2001 to 2002, he was a Research Fellow with the Nanyang Technological University, Singapore. Since 2010, he has been a Full Professor with the School of Electronic and Information Engineering, Beihang University. His research interests include global navigation satellite system and its application.

Di Wu received the bachelor's degree from the Wuhan University of Technology, Beijing, China, in 2017. Since 2017, she has been working toward the master's degree in electronic information engineering from the School of Electronic and Information Engineering, Beihang University, Beijing, China.

Her research interest focuses on global navigation satellite system reflectometry simulation for the master's degree.